Wind tunnel testing of scaled wind turbine models: Beyond aerodynamics

Carlo L. Bottasso [a,b,*], Filippo Campagnolo [b], Vlaho Petrović [c]

[a] Wind Energy Institute, Technische Universität München, D-85748 Garching b. München, Germany
[b] Department of Aerospace Science and Technology, Politecnico di Milano, Milano, Via La Masa 34, 20156, Italy
[c] Faculty of Electrical Engineering and Computing, University of Zagreb, Unska 3, 10000 Zagreb, Croatia

Article history:
Received 8 July 2013
Received in revised form
14 January 2014
Accepted 26 January 2014
Available online 22 February 2014

1. Introduction and motivation

The understanding and simulation of the wind energy conversion process for single wind turbines and wind farms requires the ability to model multiple complex interacting physical processes taking place at diverse spatial and temporal scales. Clearly, the ability to effectively design wind energy systems ultimately relies, apart from an appropriate knowledge of the physics, on the fidelity to reality of the mathematical models used in simulations. Consequently, there is a need to validate such models and to calibrate their parameters so as to maximize their accuracy.

Validation and calibration can be performed with the help of experimental observations, conducted either on the full system or on its sub-components. When looking at the full wind turbine or wind farm system, testing and measurements conducted in the field, although invaluable, present some hurdles. First, it is usually difficult to have complete and accurate knowledge of the environmental testing conditions, which by the way cannot in general be controlled, and, secondly, costs and testing time are often quite relevant.

* Corresponding author at: Wind Energy Institute, Technische Universität München, D-85748 Garching b. München, Germany. Tel.: +49 (0) 89 289 16680.
E-mail address: carlo.bottasso@tum.de (C.L. Bottasso).

To complement, support and, when possible, replace field testing, one can resort to the use of scaled models. In such testing conditions it is usually impossible to exactly match all relevant physics due to limitations of the scaling conditions, because of the frequent impossibility of assuring the same full scale and scaled values for all non-dimensional parameters. On the other hand, one has in general a better control and knowledge of the testing conditions, errors and disturbances. Furthermore, it may be possible to perform measurements which might not be feasible at full scale, and the testing typically incurs in much lower costs. Therefore, scaled testing does not replace simulation or field testing, but works in synergy with both towards the goal of delivering validated and calibrated numerical simulation tools, as well as an improved knowledge of the problem at hand.

In the area of aerodynamics, wind tunnel testing of wind turbine models has been reported by, among others, Oku et al. (1996), Hand et al. (2001), Vermeer et al. (2003), Snel et al. (2007) and Schepers and Snel (2007). These and similar studies have produced valuable information and measurements regarding the performance of rotors and the behavior of airfoils, blades and wakes, helping not only with the understanding of the aerodynamical physical processes, but also with the validation and calibration of suitable mathematical models.

Nomenclature

a	speed of sound
c	blade chord
g	gravitational acceleration
i	current intensity
n	scale factor
n_t	time ratio
r	radial position
t	time
t_f	fault time instant
A	rotor area
C_D	drag coefficient
C_F	thrust coefficient
C_L	lift coefficient
C_P	power coefficient
C_T	torque coefficient
$C_{L,\alpha}$	lift curve slope
I	blade flapping inertia
J	optimization cost function
R	rotor radius
T_a	aerodynamic torque
T_g	generator torque
V	wind speed
V_r	rated wind speed
$\boldsymbol{a}$	vector of model coefficients
$\boldsymbol{m}$	vector of blade harmonics
$\boldsymbol{p}$	vector of unknown parameters
β	blade pitch angle
λ	tip speed ratio
μ	air viscosity
ω	pulsation
ϕ	wind misalignment angle
ρ	air density
τ	non-dimensional time
Ω	rotor angular speed
Fr	Froude number
Lo	Lock number
Ma	Mach number
Re	Reynolds number
$(\cdot)^T$	transpose
$(\cdot)^{\mathrm{IP}}$	rotor in-plane component
$(\cdot)^{\mathrm{OP}}$	rotor out-of-plane component
$(\cdot)_M$	quantity pertaining to the scaled model
$(\cdot)_P$	quantity pertaining to the physical full scale system
$(\cdot)_{1c}$	first cosine harmonic
$(\cdot)_{1s}$	first sine harmonic
$(\cdot)_{fa}$	fore-aft component
$\tilde{(\cdot)}$	experimentally measured quantity
$\hat{(\cdot)}$	quantity obtained by simulation
$\dot{(\cdot)}$	derivative w.r.t. time, $\mathrm{d}\cdot/\mathrm{d}t$
ADC	actuator duty cycle
BEM	blade element momentum
CAN	controller area network
CFD	computational fluid dynamics
DLC	dynamic load case
EOG	extreme operating gust
FBG	fiber Bragg grating
FEM	finite element method
IPC	individual pitch control
LES	large eddy simulation
PID	proportional integral derivative
RANS	Reynolds-averaged Navier–Stokes
TSR	tip speed ratio

Nonetheless, aerodynamics is only one of the coupled phenomena that take place in the wind energy conversion process and whose understanding is crucial for the most effective design and operation of wind turbines. In fact, design loads on wind turbines are dictated by transient phenomena, where the effects of inertial and elastic loads, as well as of the closed-loop control laws used for a variety of tasks onboard the machine, play a very major role.

In this paper we propose to expand scaled wind tunnel testing beyond the sole domain of aerodynamics. To this end, we describe an aeroelastically scaled model of a multi-MW wind turbine, featuring active individual blade pitch and torque control. The model was designed so as to deliver realistic aerodynamic performance, and can be used for aerodynamic investigations, for example regarding wakes, their characteristics and their modeling. However, the model was also conceived for conducting experimental investigations on the aeroservoelasticity of wind turbines in the controlled environment of a wind tunnel. As such, it can be used for studying the machine response in extreme operating conditions (e.g., emergency shutdowns, operation at high yaw angles, response following failures of onboard sub-systems, etc.), something that is difficult to do in the field. The model can also support research on advanced pitch-torque control laws, on load and wind observers, as well as a variety of other aeroelastic investigations such as the study of the effects of loads induced within a wind farm by wake impingement caused by upstream wind turbines.

The paper is organized according to the following plan. Section 2 describes the scaled wind turbine model characteristics. At first, Section 2.1 describes the wind tunnel of the Politecnico di Milano where the model is typically operated. Next, Section 2.2 states the design requirements that stem from the diverse non-standard applications that need to be supported by the model, while Section 2.3 formulates the scaling laws. The general configuration of the model is given in Section 2.4, followed by Section 2.5 that describes the aerodynamic design, while Sections 2.6–2.8 describe sensors and the pitch and torque systems. The description of the model is complemented by Section 2.9 that discusses the real-time control and model management system, Section 2.10 that defines support tools that were designed for the testing, calibration and maintenance of the models and of their principal sub-components, and finally Section 2.11 that describes a comprehensive aeroservoelastic simulation environment of the experimental facility. Next, a number of non-aerodynamic and non-standard applications are presented in Section 3. A wind misalignment estimator, used in support of active yaw control, is validated in Section 3.1. Next, Section 3.2 describes the optimization of emergency shutdown maneuvers, including the calibration of a suitable mathematical model. Finally, Section 3.3 describes active control applications, focusing on regulation in wake interference conditions, as well as higher harmonic individual blade pitch control. Conclusions and an outlook to future work end the paper at Section 4.

2. Scaled wind turbine model

2.1. The Politecnico di Milano wind tunnel

The wind tunnel of the Politenico di Milano, which was used for all tests carried out during this project, is a closed-return configuration facility arranged in a vertical layout with two test rooms in the loop, as depicted in Fig. 1.

The wind tunnel features 14 driving fans for a total installed power of 1.4 MW, and has two test sections.

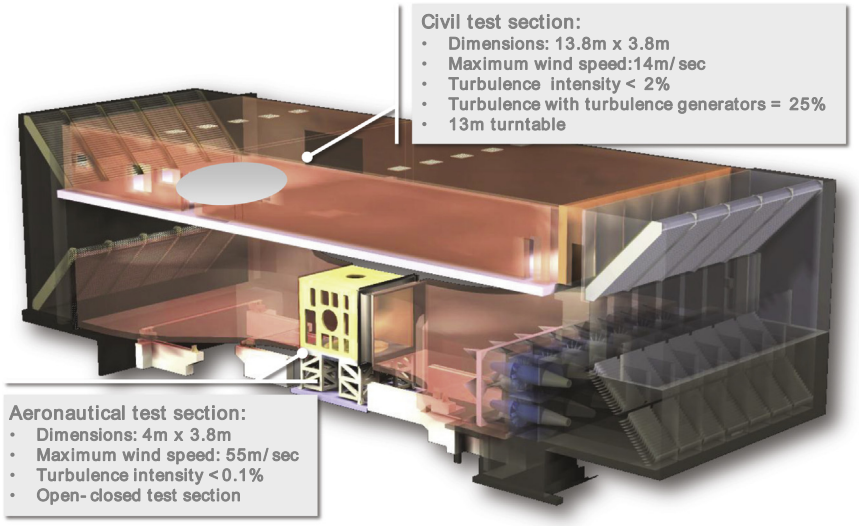

Fig. 1. Configuration of the wind tunnel of the Politecnico di Milano.

The first one — mostly used for aeronautical engineering and sports-related applications — is a low turbulence ($<0.1\%$) test section, which is located at the lower level of the facility building and placed between the contraction cone and the diffuser. The low turbulence test chamber has a maximum flow velocity of 55 m/s, a cross-sectional area of 4 m $\times$ 3.84 m and a length of 6 m. Tests can be conducted in both closed and open jet conditions.

The second test section — primarily used for civil, environmental and wind power engineering applications — is a boundary layer one, situated in the return duct at the upper level of the facility building. The test chamber has a maximum flow velocity of 14 m/s and a cross-sectional area of 13.84 m $\times$ 3.84 m with a length of 36 m, which enables tests on relatively large models with low blockage effects. Atmospheric boundary layer conditions can be simulated by the use of turbulence generators placed at the chamber inlet and of roughness elements located on the floor. A turntable of 13 m of diameter allows for the model to be yawed with respect to the incoming wind.

The wind tunnel is equipped with a complete array of devices for measuring mechanical and fluid dynamics quantities, as needed for conducting the various experiments.

2.2. *Design requirements*

For the present project, models were designed with the goal of supporting experimental observations not only in the field of aerodynamics but also in the areas of aeroelasticity and control, for single and interacting wind turbines. The need to support these diverse applications dictated a number of specific design requirements, which include

- A realistic energy conversion process enabled by good aerodynamic performance at the airfoil and blade level, translating into reasonable aerodynamic loads and damping, as well as wakes of realistic geometry, velocity deficit and turbulence intensity.
- Aeroelastic scaling, i.e. the ability to represent the mutual interactions of aerodynamic, elastic and inertial forces, which implies the realization of a flexible machine with given specific stiffness and mass properties. For a wind turbine, this also implies the ability to match the relative placement of the principal natural frequencies (of rotor, drive-train and tower) with respect to the harmonic per rev excitations, so that both the reference full scale and scaled machines have the same Campbell diagram in the lowest frequency range.
- Individual blade pitch and torque control, so as to enable the testing of modern control strategies, with appropriate bandwidth and a reasonable rendering of the principal dynamic effects of servo actuators, mainly due to time delays and maximum attainable rates.
- A comprehensive onboard sensorization of the machine, giving the ability to measure loads, accelerations and positions (e.g., blade pitch and rotor azimuth), with sufficient accuracy and bandwidth. The onboard sensorization is complemented by off-board automated traversing systems used for characterizing the flow field upstream and downstream of the machines.
- Dimensions of the models as large as possible, to avoid too low a Reynolds number, but also to avoid excessive miniaturization, which would complicate the realization of active control capabilities and the need for a comprehensive sensorization. On the other hand, the rotor dimension should not cause excessive blockage effects due to interference with the wind tunnel walls, and should allow for the testing of at least two wind turbines in wake-interference conditions, capable of representing the typical couplings taking place within a wind farm between and among wind turbines.

The scaled models were loosely based on the Vestas V90 wind turbine, a 3 MW machine with a 90 m diameter rotor and a hub height of about 80 m. Based on the minimum cross-sectional dimensions of the wind tunnel test chambers, the scaled model rotor diameter was chosen to be equal to 2 m, leading to a geometric scaling factor of 1/45. This dimension avoids excessive blockage, and still allows for the testing in the boundary layer test section of two wind turbines one in front of the other at distances of about 4–5 rotor diameters.

The models were complemented by a number of custom designed devices used for their characterization, calibration and off-line pre-testing outside of the wind tunnel. Furthermore, a comprehensive simulation environment of the experimental facility was developed, including aeroservoelastic multibody models of the wind turbine as well as CFD models of the coupled machine–wind tunnel environment. The simulation models supported the design and testing phases, and were validated and calibrated with the use of experimental data gathered in the wind tunnel, as described later on in this work.

2.3. Scaling laws

The non-dimensional parameters governing the dynamics of wind turbines can be derived with the help of Buckingham Π Theorem (Buckingham, 1914; Barenblatt, 1996), and are represented by the tip-speed-ratio (TSR) $\lambda = \Omega R/V$, where Ω is the angular speed of the rotor of radius R and V is the wind speed, the Reynolds number $\mathrm{Re} = \rho V c/\mu$, where ρ is the density of air, c is a characteristic length and μ is the fluid viscosity, the Froude number $\mathrm{Fr} = V^2/gR$, where g is the acceleration of gravity, the Mach number $\mathrm{Ma} = V/a$, where a is the speed of sound, and the Lock number $\mathrm{Lo} = C_{L,\alpha}\rho c R^4/I$, where $C_{L,\alpha}$ is the slope of the lift curve and I is the blade flapping inertia, as well as the non-dimensional natural frequencies $\widetilde{\omega}_i = \omega_i/\Omega$, and non-dimensional time $\tau = \Omega t$, with t indicating time.

Scaling laws were here derived based on two criteria.

The first requires the exact enforcement between the full scale and scaled models of the same values of TSR (which amounts to having the same aerodynamic kinematics), of the same Lock number (which amounts to having the same ratio of aerodynamic to inertial forces), and of the same non-dimensional natural frequencies (which amounts to having the same relative placement of natural frequencies and harmonic excitations), or, in symbols

$$\lambda_M = \lambda_P, \quad \mathrm{Lo}_M = \mathrm{Lo}_P, \quad \widetilde{\omega}_{i_M} = \widetilde{\omega}_{i_P}, \tag{1}$$

where $(\cdot)_M$ indicates quantities referred to the scaled model, and $(\cdot)_P$ indicates quantities referred to the physical full scale one.

The second criterion is to look for the best compromise between the contrasting requirements of limiting the Reynolds mismatch $\mathrm{Re}_M/\mathrm{Re}_P$, which is related to the quality of the aerodynamics of the scaled model, and the need to limit the speed-up of scaled time t_M/t_P, in order to avoid an excessive increase in the control bandwidth. In fact very high control frequencies, made necessary by an excessively fast scaled time, would make it difficult to test advanced control laws, which is one of the goals of the project, since such laws might possibly imply a non-negligible number of operations but would still need to be operated in real-time on the model.

The design of best compromise between these two requirements can then be expressed as the following minimization problem:

$$\min_{n_t}\left(k^2\frac{\mathrm{Re}_M}{\mathrm{Re}_P}+\frac{t_M}{t_P}\right) = \min_{n_t}\left(\frac{k^2 n^2}{n_t}+n_t\right), \tag{2}$$

where $n_t = t_M/t_P$ is the time ratio, $n = R_M/R_P = 1/45$ is the length scale factor, so that the Reynolds ratio is $\mathrm{Re}_M/\mathrm{Re}_P = n^2/n_t$; finally, k is a weight factor in the objective function, chosen in the present case to be equal to the value of 2. The solution to problem (2) is readily found to be $n_t = kn$.

By this definition of the scaling, one finds a mismatch in the representation of the Reynolds number equal to $\mathrm{Re}_M/\mathrm{Re}_P = n/k$, which in the present case is equal to 1/90; the effects of such a reduced Reynolds number on the model can be partially compensated, as discussed later on, by the use of special low-Reynolds airfoils augmented by transition strips. Similarly, the Froude mismatch is $\mathrm{Fr}_M/\mathrm{Fr}_P = 1/(nk^2)$, i.e. 11.25 in this case; the effects of a mismatched Froude are important only for very large wind turbines, where gravity plays a relevant role. Finally, the Mach mismatch is $\mathrm{Ma}_M/\mathrm{Ma}_P = 1/k$, i.e. 0.5 in this case; although compressibility effects do not play a role at the tip velocities of both the full scale and scaled machines, it is interesting to notice that Mach scaling corresponds to the optimization-based one defined by Eq. (2) for the case $k=1$.

2.4. General configuration

The general arrangement of the scaled wind turbine model is shown in Fig. 2, while Fig. 3 shows a view of the rotor–nacelle assembly.

The blades are mounted on the hub with two bearings, to avoid any flapwise or edgewise free-play, and house in their hollow roots zero-backlash pitch motors with built-in relative encoders. Aeroelastically scaled blades are realized using a machined Rohacell core, which ensures the right shape to the variable chord and twist blade, and two spar caps made of unidirectional carbon fiber, whose width and thickness were optimized to achieve the right stiffness. The blade surface is covered with a polymeric layer that closes the pores of the Rohacell core and ensures a smooth finish. Multiple load measurement points along the span are provided by

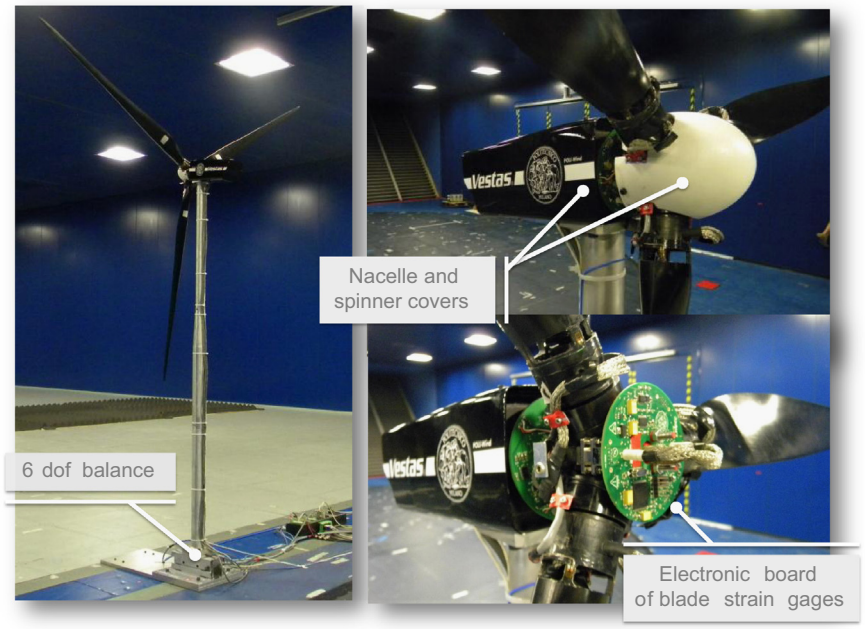

Fig. 2. General arrangement of the scaled wind turbine model.

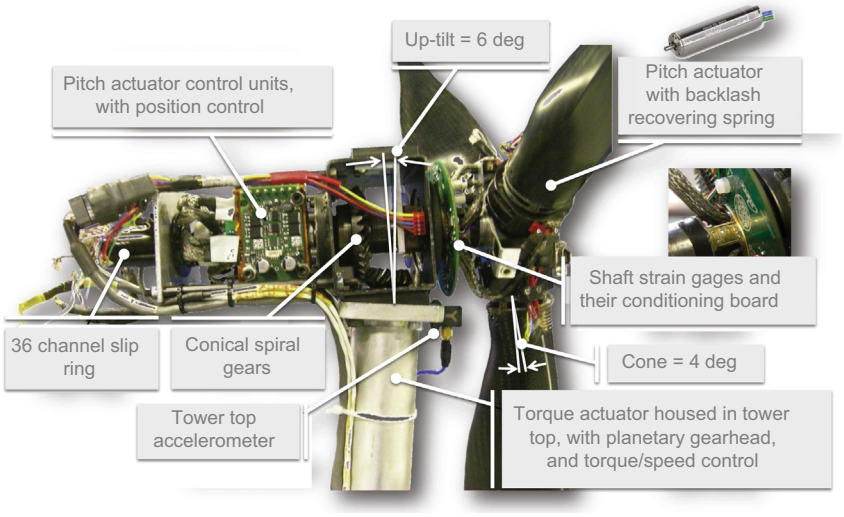

Fig. 3. View of the rotor–nacelle assembly.

Fiber Bragg Grating (FBG) sensors (Hill and Meltz, 1997), integrated in the spar caps. Further details on the design, manufacturing and characterization of the aeroelastically scaled blades are given in Campagnolo (2013).

Non-aeroelastic, i.e. rigid, blades were also manufactured using carbon fiber, and are shown in the figures. To measure blade root bending, a machined steel component, inserted at the blade root during the curing process, is composed of four small bridges, sized so as to exhibit sufficiently high load-induced strains to achieve the necessary level of accuracy of the strain gages, which are mounted on the same bridges.

The shaft was also machined for a similar reason, and hosts strain gages that measure the torsional and bending loads. Additionally, the shaft was sized so as to match the placement of the first torsional frequency of the reference machine drive-train. Two electronic boards, one in front (cf. Fig. 2) and one behind (cf. Fig. 3) the hub, provide for the power supply, conditioning and A/D conversion of, respectively, the blade root and shaft strain gages.

The shaft is mounted on two bearings, held by a rectangular carrying box that constitutes the main structural member of the nacelle. Here an optical relative encoder measures the azimuthal position of the shaft, while a triaxial accelerometer provides for measurements of the acceleration in the nacelle, used for triggering emergency shutdown procedures and optionally for control purposes. A pair of conical spiral gears, with a 2/1 reduction ratio, connects the shaft with a motor that provides for the torque (and optionally speed) control of the rotor. The torque motor is housed in the top of the tower; compressed air is blown in at the tower foot and, traveling along the hollow tower, cools the torque motor, before escaping from a small hole in the back part of the tower top.

Behind the nacelle carrying box, the three electronic control boards of the pitch actuators are mounted on the shaft and therefore rotate with it. A 36-channel slip ring occupies the aft part of the nacelle, held in place by a plate connected to the main carrying box by four rods.

The tower is realized with a tube whose stiffness was designed so that the first fore-aft and side-side natural frequencies of the nacelle-tower group of the scaled model match the scaled ones of the full scale system; since the mass of the nacelle is higher than the scaled mass of the real wind turbine, the tower stiffness is higher than the scaled stiffness of the real tower. At the foot of the tower, the model is mounted on a balance (see Fig. 2) that provides measurements of the three force and three moment components at the tower base.

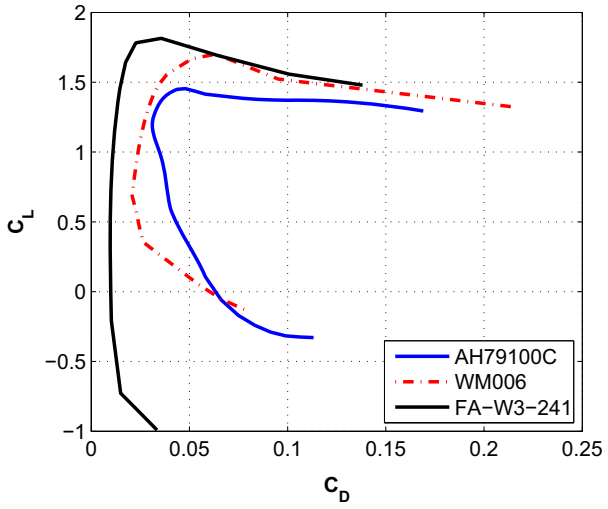

Fig. 4. Polars of the low-Reynolds airfoils AH79-100C and WM006 at $\mathrm{Re} = 6 \times 10^4$, and of the FA-W3-241 airfoil at $\mathrm{Re} = 12 \times 10^6$.

Finally, aerodynamic covers of the nacelle and hub ensure a satisfactory quality of the flow in the central rotor area.

2.5. Model aerodynamics

The average chord-based Reynolds number, which on the V90 is in the range $4–5 \times 10^6$, on the scaled model is only in the range $5–6 \times 10^4$. To account for such large differences, the blade was designed using the special low-Reynolds airfoils AH79-100C (Althaus, 1988) and WM006 (Olesen, 2009), whose polars are reported in Fig. 4; for comparison purposes, the same figure reports also the polar of the FA-W3-241 airfoil at $\mathrm{Re} = 12 \times 10^6$, a profile commonly adopted in the outer part of multi-MW rotor blades. The plots show the higher drag produced by the low Reynolds airfoils, while similar lift coefficients are observed for both low and high *Re* profiles. The AH79-100C airfoil was used in the inboard section for $r/R \in [0.137, 0.423]$, while the WM006 airfoil in the outboard one for $r/R \in [0.654, 1]$. Not to alter the aerodynamic characteristics of the airfoils, interpolations of the cross-sectional shapes were limited to a relatively small transition region between the inboard and outboard sections, i.e. for $r/R \in [0.423, 0.654]$, and at the root

region to smoothly deform the inboard airfoil into the blade root cylinder.

The blade spanwise chord distribution was geometrically scaled from the one of the reference machine; on the other hand, to account for the change of airfoils between full scale and scaled blades, the blade twist was modified to yield an optimal spanwise distribution of the axial induction factor.

Reference rotor aerodynamic performance was measured by testing the model in the low-turbulence aeronautical test section of the wind tunnel, with wind speeds from 4 to 9 m/s, rotor speeds from 330 to 400 rpm, TSRs from 5 to 11 and blade pitch settings from -5° to 15°.

Transition strips were optimized with the goal of maximizing aerodynamic power. The best performing ones present variable chordwise width, obtained by using a cutting plotter to shape an adhesive tape, and variable thickness, sized by the method of Braslow and Knox (1958) and approximated by using a spanwise varying number of tape plies. The precise chordwise location of the strips was ensured by shaping with the plot cutter an adhesive paper template extending from the blade trailing edge to the aft edge of the transition strip.

The wind tunnel thrust and power data was corrected for a non-negligible wake blockage effect ($\pi R^2/A_{\text{section}} \sim 0.207$) by applying the disk actuator method proposed in Bahaj et al. (2007) and verified by RANS CFD simulations of the experiment with and without wind tunnel walls (Campagnolo, 2012). The measured power and thrust coefficients, corrected for blockage effects, are reported as functions of TSR and blade pitch in Fig. 5. The maximum power coefficient was approximately 0.4 and 0.35, respectively before and after applying blockage corrections. The thrust coefficient at $\lambda \approx 7.5$ and $\beta = -2^\circ$, i.e. the optimal rotor operating point, was approximately 0.68 and 0.62, respectively before and after applying blockage corrections.

The model aerodynamic performance in terms of its power coefficient is approximately 30% lower than that of a full-scale wind turbine, as for example the one described in Jonkman et al. (2009). However, the general shape of the $C_P - \lambda - \beta$ curves is very similar to the one of the reference machine; furthermore, their maxima are located at approximately the same values of the tip speed ratio and blade pitch. The thrust coefficient curves are on the other hand extremely similar to the reference machine. The aerodynamic performance of the model therefore appears to be sufficiently realistic for the purposes of the present study.

Significant differences were observed between the experimentally measured and theoretical BEM-based rotor aerodynamic performance, computed using the nominal airfoil polars obtained by other authors from wind tunnel measurements. To correct for such differences, an identification process was developed that, taking as input measured rotor power and thrust coefficients at different TSR and blade pitch values, produced corrections to the nominal polars computed so as to minimize the difference between measured and BEM-computed power and thrust coefficients (Campagnolo, 2012). This procedure was used because the small size of the blade prevented the direct local measurement of airfoil aerodynamic characteristics by pressure taps or other means. The improved polars were then used in the definition of aeroservoelastic and LES lifting line models of the scaled wind turbine model.

2.6. Onboard sensors

Onboard sensors are used for collecting data on the behavior and response of the model during experimental observations, for loop-closure by the wind turbine control system, and by the supervisory controller for switching among different machine states as well as for handling emergencies.

The rotor azimuthal position is measured by an optical incremental encoder with $N_p = 1800$ counts per revolution; a zero-index track is used for providing the absolute rotor azimuth. The quadrature signal is read in 4X counting mode, and the rotor speed is computed based on the number of observed pulses within a time window $T_{\text{sc}} = 4$ ms, with a quantization error that at rated rotor speed is equal to $E_\Omega = 60/\Omega N_p T_{\text{sc}} \simeq 0.57\%$.

Shaft load measurements are obtained by strain gages mounted on small bridges, machined directly from the hollow shaft just aft of the hub and sized so as to be subjected to sufficiently high strains. These load transducers were calibrated by using dead weights to stress the shaft simultaneously with torque and two bending moment components. A full 3-by-3 sensitivity matrix was obtained by linear regression, leading to the good quality measurements shown in Fig. 6(a).

Blade root load transducers, again obtained by using strain-gages mounted on suitably deformable bridges, were similarly calibrated using known dead loads. After having verified the insensitivity of the transducer measurements to axial and torsional loading conditions, a full 2-by-2 sensitivity matrix was obtained by linear regression, leading to the quality of measurements shown in Fig. 6(b).

Global loads on the machine are measured with a `RUAG SG 192-6I` balance (http://www.ruag.com) placed at the tower foot, with an accuracy of about $\pm 0.3\%$ of the scale limit.

Accelerations at the nacelle are measured by a `PCB 356A17` triaxial accelerometer, and used by the supervisory system to trigger shutdowns when a threshold of 2 g is reached. Finally, two

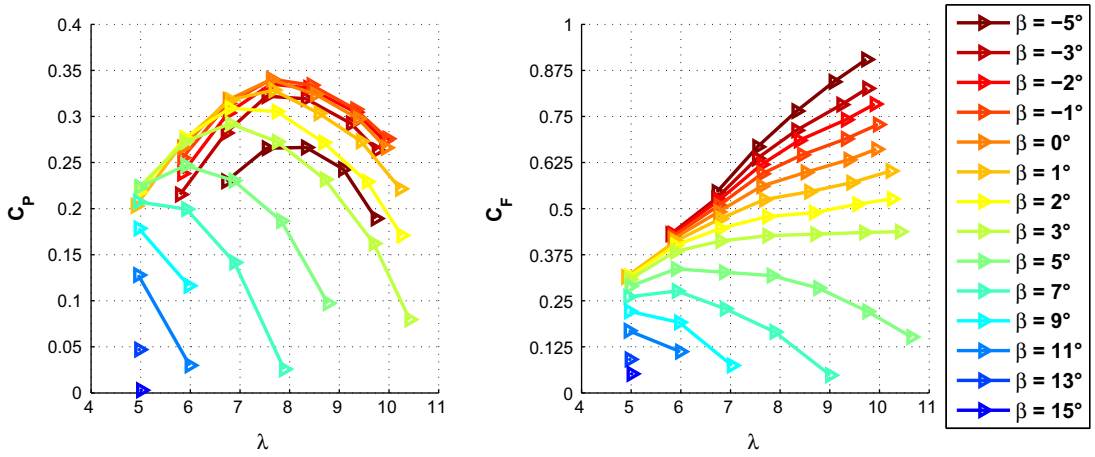

Fig. 5. Measured power C_P and thrust C_F coefficients, corrected for blockage effects, as functions of TSR and blade pitch.

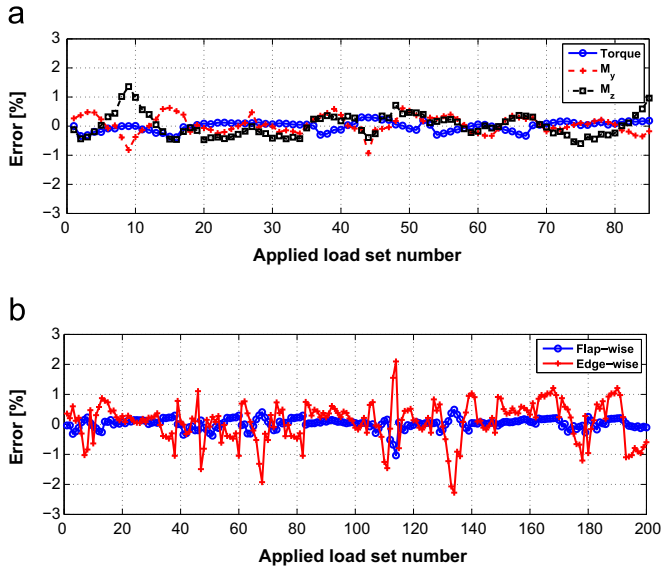

Fig. 6. Errors between known applied loads and strain-gage measured ones, in percent of reference loads of typical operating conditions, for the load transducers at the shaft (top) and at the root of one of the blades (bottom).

Pt100 probes are used for monitoring the winding and gearhead temperature of the torque actuator, with the supervisory system programmed to change the model state from power production to idling in the case of generator overheating.

2.7. Pitch system

The Faulhaber 1724T018SR brushed motor, equipped with a 16/7-134:1 precision gearhead and IE2-512 encoder (http://www.faulhaber.com), was selected as the pitch actuator on the basis of requirements for accuracy and repeatability of pitch positioning, compatibility of dimensions with the housing space available at the blade root, a sufficiently high maximum pitch rate to allow for the simulation of emergency shutdown operations, and a sufficiently wide bandwidth to ensure individual pitch control capabilities. The gearhead backlash ($\sim 1^\circ$) was removed by using a torsional spring connecting blade root and rotor hub. Spring stiffness and assembly position were designed so as to have a restoring torque, with the blade positioned at 0° pitch, equal to about half of the maximum torque supplied by the pitch motor.

Each pitch actuator is driven by its own MCDC3003C control board (http://www.faulhaber.com), with the three boards of the three pitch motors being nodes of the same Controller Area Network (CAN). The boards receive–transmit data at 500 kb/s from-to the real-time control unit using the CANopen communication protocol; this has the advantage, with respect to the standard serial communication, of reducing the required number of slip ring channels. The pitch angle can be set individually for each blade by appropriately sending the desired pitch value to each control board; in turn, this quantity represents the reference input of two PID controllers for speed and position implemented on the control boards, whose gains were set by the open-loop Ziegler–Nichols (1942) method. Feedback is based on the motor built-in encoder measures.

The pitch actuator performance was verified by replacing the blade with a cylindrical short dummy element, featuring the same pitch inertia. The effective pitch angle was measured by using a flexible linear strip potentiometer fixed at the blade root (see Fig. 9 (a)), whose relationship between voltage output and pitch angle was previously determined by measuring the latter with an extremely accurate (± 1 arcmin) WYLER CLINOTRONIC PLUS inclinometer. Static tests confirmed a good repeatability and an acceptable accuracy of about $\pm 0.1^\circ$. Dynamic tests were then used to identify the transfer function $H(s) = \beta(s)/\beta_{\text{ref}}(s)$ between reference β_{ref} and measured β pitches; the resulting actuator natural frequencies and damping ratios are given in Table 1. The bandwidth of the pitch actuator is around 30 Hz, i.e. approximately five times the 1P pulsation, and quite similar to the bandwidth of typical multi-MW pitch actuators.

Table 1
Pair poles of the identified pitch actuator transfer function.

Pair poles	Frequency (Hz)	Damping ratio
First pole	32.5	0.25
Second pole	19.6	0.85

2.8. Torque actuator

The Maxon EC-4-Pole-30BL-200W brushless motor, equipped with a GP32HP-14/1 gearhead and MR-500IMP magnetic encoder (http://www.maxonmotor.com), was selected as the torque actuator on the basis of requirements for rotational speed, compatibility of dimensions with the housing space available at the top of the tower, and a maximum power slightly higher than the scaled one of the reference wind turbine.

The torque actuator is driven by the 4-Q-EC-DES-50/5 control board (http://www.maxonmotor.com), which allows us to operate the motor also as a generator. The produced electrical power is dissipated by using a 12–75 V/5.0 Ω shunt regulator chopper connected to an external 6 Ω resistance, capable of dissipating a continuous power of up to 300 W.

The actuator can be controlled in speed or torque mode. Speed control is performed by appropriately sending the desired reference speed to the control electronics by using the CANopen communication protocol at a data transfer rate of 500 kb/s. The gains of the 4-Q-EC-DES-50/5 internal PI speed controller, which uses the motor encoder measure as feedback signal, were set to achieve a good speed reference tracking with a low level of speed and current oscillations.

Usually, for small size wind tunnel models, torque control is implemented in open loop, by forcing the actuating system to supply a desired current value i, related to the generator/motor torque T_g via the linear relationship $T_g = K_T i$, under the assumption of a constant proportionality parameter K_T. However, this approach works only when the electrical device operates in a restricted range of speed–temperature and when there are no mechanical moving parts interposed between the actuator and the driven system. On the other hand, in the present application the rotor speed varies depending on the wind speed, the temperature is subject to considerable variations during operation, and the nacelle bearings and gearhead provide variable and difficult-to-predict friction torques. Therefore, a closed-loop torque controller was implemented onboard the real-time monitoring system of the model (see later on Section 2.9). The controller uses the shaft torque measurement as feedback signal, and sends a current reference to the motor control electronics via its analogue input every 400 μs.

The main objectives of the controller are an accurate tracking of the reference torque and an extremely fast response of the actuator against variations of the same reference. Indeed, torque response is typically quite fast for real multi-MW wind turbines, with time constants of the order of 0.01–0.02 s. However, in the present case the requirement of a fast response was found to be hampered by the not negligible oscillations observed in the shaft torque measurements, especially at higher rotor speed and torque

levels. The source of the oscillations was traced back to the not perfectly homogenous meshing of the bevel gear teeth, with a consequent excitation of the shaft natural modes and resulting high frequency oscillations with amplitudes of the order of about 10% of the mean value.

To correct this problem, the feed-forward control scheme shown in Fig. 7 was developed; such an approach allows one to independently design the system response for reference changes and for disturbance rejection (Ogata, 1997). The formulation is based on the linear model

$$T_g = a\Omega + bu + c, \tag{3}$$

where T_g is the generator torque, u is the current reference sent to the generator control electronics (i.e. the controller output). Model parameters a, b and c are determined from steady state measurements performed on the back-to-back test bench described in Section 2.10, which allows one to independently set both generator torque and speed. The generator torque T_g, rotor speed Ω and current reference u were recorded over the whole operating regime, and the model parameters were calculated by a least squares fit.

Because of the integral behavior of the PI controller, the offset c is not necessary for control, and the actual feed-forward term is computed as

$$u_{FF} = \frac{1}{b}T_{g,r} - \frac{a}{b}\Omega, \tag{4}$$

where $T_{g,r}$ is the torque reference. Assuming well tuned model parameters in Eq. (3), the feed-forward term guarantees a fast torque response when the reference changes. Therefore the PI controller, whose main purpose is to compensate the disturbances caused by slow temperature changes and to ensure an offset-free reference tracking, does not have to be very fast. This way one can low-pass filter the feedback measurement, thereby eliminating the disturbing oscillations, in the end ensuring an accurate and fast torque control performance.

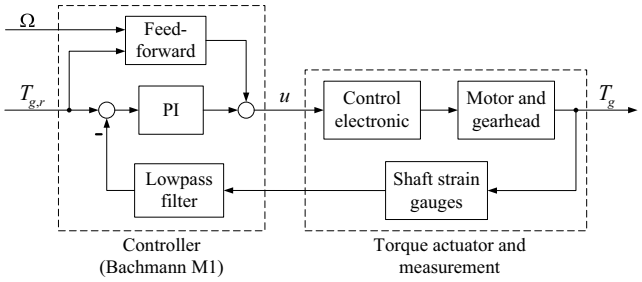

Fig. 7. Torque control scheme.

2.9. Real-time control and model management system

The architecture of the data acquisition, control and management system is shown in Fig. 8. The experimental model is controlled by a hard-real-time module implementing a supervisor of the machine states and pitch-torque control laws, similar to what is done on a real wind turbine. Two implementations of this system were developed, one using a real-time patch of the Linux operating system (https://www.rtai.org) running on a standard PC, and the other based on the industrial `Bachmann M1` system (http://www.bachmann.info), which was used in all tests reported in this paper and that therefore will be described in the following paragraphs.

Three analog acquisition modules and one counter module acquire all model onboard sensors, as well as the wind tunnel ones (including wind speed, air temperature and humidity), at a sampling frequency of 250 Hz. Shaft loads and tower top accelerations are filtered with an 8th-order analog Butterworth filter and then sampled at 2.5 kHz.

All sensor readings are provided as inputs to the supervision and control algorithms, which is executed in real-time on the `M1 CPU` unit every 8 ms. The controller outputs are represented by pitch and torque demands, which are sent to the actuator control boards via the `M1 CAN` module or by analog output.

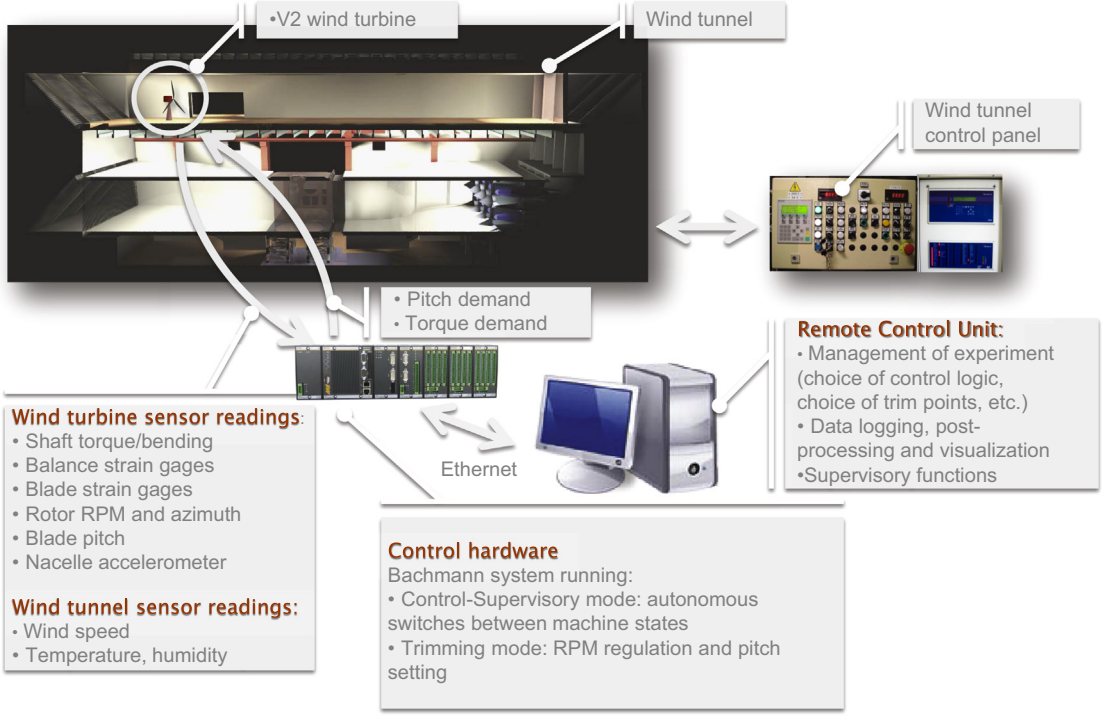

Fig. 8. Data acquisition, control and model management system.

The supervision control system switches among different possible machine states (parking, power production, shutdown, run up, etc.) either in an autonomous way, for example in the case of emergencies triggered by excessive rotor speed or by the overheating of the torque actuator, or by a direct request form the user. The control logic includes different collective or individual pitch-torque control laws, whose gains can be readily adjusted by the user, and a simple trimming mode that regulates the machine at a user-specified value of rotor speed and blade pitch.

Finally, an operator control station runs software for the management of the experiment, for data logging and visualization of all measurements through the support of dedicated graphic interfaces that allow for the rapid visualization of the results of each specific run.

2.10. Support equipment

The wind turbine aeroservoelastic experimental facility is complemented by a number of support tools for the testing, calibration and maintenance of the models and of their principal sub-components.

A back-to-back test bench, with the blades replaced by dummy ones yielding the same rotor inertia (see Fig. 9(b)), was used for the hardware-in-the-loop verification and tuning of the control-supervisory algorithms. The aerodynamic torque is computed in real-time as

$$T_a = \frac{1}{2}\rho V^2 \pi R^3 C_T(\lambda, \beta), \tag{5}$$

where $\lambda = \Omega R/V$, while Ω and β are the measured rotor speed and the blade pitch, respectively. The rotor-equivalent wind speed V is provided by a user-defined time history, while $C_T(\lambda, \beta)$ is the experimentally measured rotor aerodynamic torque coefficient stored in look-up table form, and interpolated at run time. The computed aerodynamic torque is applied to the rotor by a brushless `Maxon EC-45` motor, equipped with a `GP-42C` gearhead and `EHDL` encoder.

In addition, specific support tools were designed to guarantee an accurate calibration of the shaft and blade root strain gages, where a laser emitter was used to align the dead loads with the desired direction and for zero setting the pitch and azimuth encoders with an accuracy of $\pm 0.2^\circ$. Similarly, a small laser emitter placed at the hub center was used to precisely align the rotor axis with the wind tunnel wind direction.

2.11. Simulation environment

A comprehensive aeroservoelastic simulation environment has supported all phases of the wind turbine model design, including the determination of loads, the calculation of the response of the machine in its entire operating envelope, and the testing and tuning of control laws. Mathematical models of the full scale and scaled wind turbines were developed with the code `Cp-Lambda` (*C*ode for *P*erformance, *L*oads and *A*eroelasticity by *M*ulti−*B*ody *D*ynamic *A*nalysis) (Bottasso and Croce, 2009–2013), based on a finite-element multibody formulation (see Bauchau et al., 2001, and references therein). The full scale mathematical model was based on data provided by the sponsor, while the mathematical model of the scaled wind turbine was based on its geometric, structural and aerodynamic characteristics, including polars of the low Reynolds airfoils identified as previously explained from rotor performance data. Structural cross-sectional characteristics of the blade, including inertia as well as 6-by-6 stiffness matrices, were computed with the composite blade analysis code `ANBA` (*An*isotropic *B*eam *A*nalysis) (Giavotto et al., 1983), and verified with detailed three-dimensional FEM models when necessary.

3. Applications and results

To demonstrate the flexibility of the model in supporting diverse wind energy applications, in this section we illustrate its use for three quite different problems. The first is related to technologies in support of wind turbine control, and describes the validation of an observer that estimates wind direction based on blade loads, used for providing reliable information to a yaw controller. The second deals with the management of shutdown procedures, and the study of the effects that optimized pitch policies can have on design-driving loads. Finally, the last one deals with controls, and illustrates the regulation of wind turbines in wake interference conditions emulating operation within a wind farm, as well as the reduction of blade loads by higher harmonic individual blade pitch control. Purposely, purely aerodynamic applications are not described here, to underline that the applicability of the model extends into domains that are typically tackled only by simulation and/or field testing. Nonetheless, purely aerodynamic applications are clearly of great interest, and aerodynamic studies conducted with the equipment described here are presented in Campagnolo (2013).

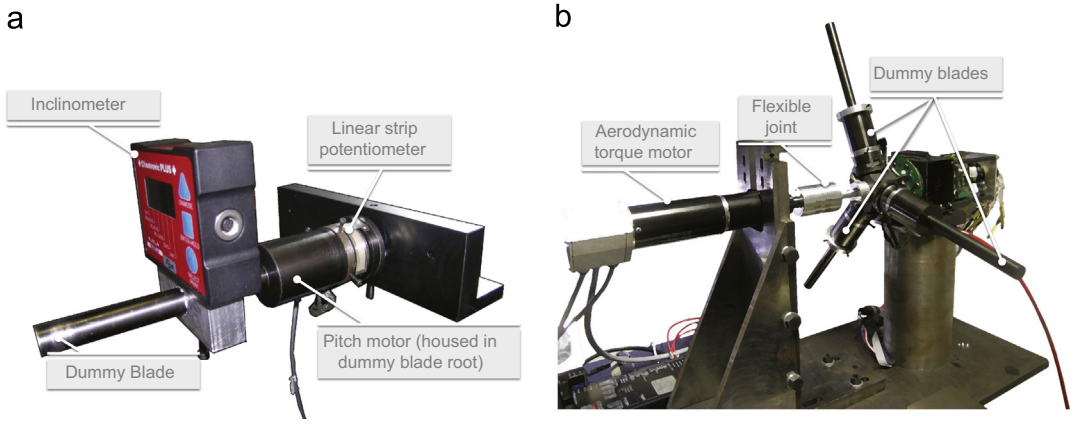

Fig. 9. Setup used for determining the pitch actuator performance (at left), and back-to-back test bench used for the hardware-in-the-loop verification and tuning of the control-supervisory algorithms (at right).

3.1. Validation of a wind misalignment estimator

Operation in yawed wind conditions reduces power output and generates undesirable loading on the machine, including the possible excitation of low damped side-side modes, with a potential increment in fatigue damage. On the other hand, actively yawing the machine has a relevant cost, since it involves the movement of the rotor–nacelle assembly, a component of extremely large mass on multi-MW wind turbines. As a consequence, yaw actuation for rotor realignment should be driven by reliable wind direction information, to maximize the efficacy of the maneuver and to limit the duty-cycle of the driving system.

Unfortunately, accurate measurement of wind misalignment is often difficult to obtain. In fact, sensors of wind direction are usually affected by various sources of inaccuracy, being typically influenced by the turbulent rotor wake and the disturbance of the flow caused by the nacelle. Even when sensors are well compensated for all sources of error, current instruments only provide a point local information, usually at hub height. A more desirable piece of information would clearly be represented by some rotor-effective wind direction, in contrast to the current local one, especially on rotors of very large swept area.

To overcome the limitations of the current technology, a novel approach based on the use of the whole rotor as a wind sensor was described in Bottasso and Riboldi (2014). The basic idea of that approach consists in using blade loads, typically measured with strain gages at each blade root, to infer the wind direction, by exploiting the effect that a lateral wind component has on the amplitude and phasing of the blade response. The same approach can also be used to infer additional wind information, as for example the vertical wind shear. Since the wind state estimates are obtained directly by the rotor response as measured by the rotor loads, the resulting information has a rotor-equivalent (as opposed to local) nature.

Bottasso and Riboldi (2014) show that wind direction and shear are observable from the blade loads by inverting the 1P response of an analytical blade flapping model. In that same work, the simplified analytical result is used to suggest the form of a more general observation model that, while maintaining the same structure of the analytically derived one, is defined in terms of unknown coefficients, which are in turn estimated by a system identification approach.

Limiting here the discussion to the sole wind direction, the observation model takes the following form:

$$\phi = \boldsymbol{a}(V)^T \boldsymbol{m}, \tag{6}$$

where ϕ is the estimated wind direction with respect to the rotor, $\boldsymbol{a}(V)$ is a vector containing the linear observation model coefficients, scheduled in terms of the wind speed V, while the driving input vector $\boldsymbol{m}$ is made up of 1P load harmonic amplitudes

$$\boldsymbol{m} = (m_{1c}^{\mathrm{OP}}, m_{1s}^{\mathrm{OP}}, m_{1c}^{\mathrm{IP}}, m_{1s}^{\mathrm{IP}})^T, \tag{7}$$

where $(\cdot)_{1c}$ and $(\cdot)_{1s}$ indicate the first cosine and sine harmonic amplitudes, respectively, while $(\cdot)^{\mathrm{OP}}$ and $(\cdot)^{\mathrm{IP}}$ indicate the out- and in-plane blade root bending moment components, respectively.

Given a wind speed V_i, having a set of sufficiently complete measurements of wind direction ϕ and associated blade root harmonics $\boldsymbol{m}$ around that same wind speed (typically, 4–6 different conditions in the present case), one may identify the model coefficients $\boldsymbol{a}(V_i)$, for example by using least squares. Next, the models obtained this way at different wind speeds are linearly interpolated at the generic wind speed V, to yield a linear parameter varying observation model covering the range of wind speeds of interest. Finally, at each time instant during operation of the machine, model (6) is used to estimate the wind direction, based on the current wind speed and blade load harmonic amplitudes. Given the fact that yaw actuation is performed only when the wind misalignment has been above a certain threshold for a sufficiently long period of time, the estimates provided by the observation model are typically filtered with a moving average to avoid responding to fast wind fluctuation and disturbances. More details on the formulation are given in Bottasso and Riboldi (2014).

The wind observer here briefly described was extensively validated using models of multi-MW wind turbines in the high-fidelity aeroservoelastic simulation environment provided by the `Cp-Lambda` code, which however still represents only a simplified model of reality. On the other hand, the field testing of the observer presents numerous challenges, including the difficulty of finding and having access to synchronized time sequences of wind direction measurements, for example obtained by a met mast at various heights, and associated blade loads.

The experimental facility described in this paper provides for an ideal way of conducting an experimental verification of the wind observer. In fact, all necessary measurements are available onboard the model, including blade loads and rotor azimuth (necessary so as to compute the load harmonics). Furthermore, the wind conditions in terms of speed and direction are easily controllable, the latter parameter being readily changed by simply bolting the model to the wind tunnel floor at the desired angles with respect to the wind tunnel axis, as shown in Fig. 10.

The observation model coefficients $\boldsymbol{a}(V)$ were identified from trials conducted in the range $\pm 30^\circ$ of misalignment angles, with a spacing of 10° between trials. All runs were performed at the same tip speed ratio corresponding to a full power condition, with a constant rotor speed of 365 rpm, a mean hub wind speed of 8.5 m/s, and a fixed pitch value of 5.35°. Since in the wind tunnel the vertical shear cannot be changed quickly during an experiment, tests were performed with a single fixed value of shear. This limitation does not affect the present results, because the independence of shear on misalignment, and vice versa, had been previously verified by simulation (Bottasso and Riboldi, 2014). For each trial, loads were recorded for 30 s, filtered with a zero-phase 4th-order Butterworth low-pass filter to lower the noise level; finally, load harmonics were computed by projection on a demodulation window of 15 rotor revolutions.

The synthesized observer was then used for estimating wind misalignment. The observer was fed by blade loads measured in wind tunnel runs characterized by the same values of all

Fig. 10. Setup for the experimental validation of the wind direction observer. Notice how the model, which at present does not feature active yaw control, is bolted to the floor at an angle with respect to the wind direction to realize a wind misalignment condition.

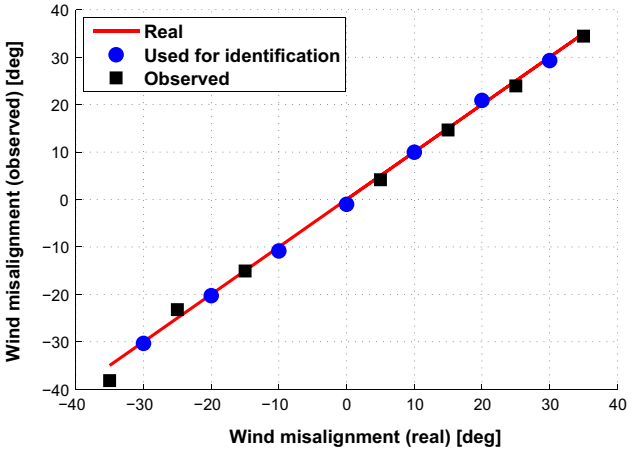

Fig. 11. Comparison of the average observed wind misalignment angle with respect to the true one, i.e. the model mounting angle.

parameters used in the estimation phase, but with different misalignment angles, set in the range $\pm 35^\circ$ with a step of 10° between trials.

The results are reported in Fig. 11, which plots the observed wind misalignment vs. the true one, i.e. the model mounting angle with respect to the wind tunnel axis, as measured with a laser emitter mounted in the hub. The results confirm, on the one hand, the good quality of the estimates provided by the observer — results that further support the conclusions drawn from an extensive simulation campaign — and on the other the potential offered by the present aeroservoelastic experimental facility as a tool for the validation of wind turbine control support technologies.

3.2. *Emergency shutdown: maneuver optimization and model calibration*

The present model was designed so as to be able to simulate in the wind tunnel, among other things, those emergency conditions that, although rarely occur in the lifetime of the machine, may define the envelope loads in some of its principal components. A typical case is represented by the tower, whose sizing loads are often dictated by the effects produced by an extreme gust with simultaneous grid loss at wind speeds close to rated (DLC 1.5(a), see IEC, 2005), with the consequent loss of electrical torque and no onboard measurements available for feedback.

Indeed, it appears that the optimization of the control strategy during emergencies has not yet been the subject of an intense interest in the scientific literature. This is unfortunate, because the reduction of envelope loads can be readily translated into savings by resizing the affected wind turbine components, especially if the next dominating non-emergency-related loads are significantly lower.

In the present section, we show how wind tunnel testing can be used for simulating, at least in part, shutdown maneuvers and how, after having calibrated the mathematical model of the machine with the help of experimental data, one can use that same model to study the effects of different pitch profiles with the goal of minimizing loads.

Unfortunately, it is difficult to exactly replicate in the wind tunnel the typical conditions prescribed by the certification guidelines during emergencies. In fact, the generation, for example, of a typical "Mexican hat" Extreme Operating Gust (EOG, see IEC, 2005) implies substantial changes in the wind speed within about 10 s. Given Eq. (2), which implies a scaling of time $n_t = kn = 2/45$, this would require the ability to substantially change the wind tunnel longitudinal flow speed in about half a second, something that is not easily done for such a large wind tunnel as the one used here. In fact, the high fluid inertia prevents the use of the wind tunnel driving fans to produce the required high flow accelerations. A possible solution would be the use of suitable longitudinal gust generators, which however were not available during the conduction of this study.

Notwithstanding such limitations, the wind tunnel testing of shutdown procedures can still provide useful information to the analyst. To illustrate this point, we performed the following tasks. At first, we defined different open-loop control policies for the pitch actuation during shutdowns, and we tested them in the wind tunnel using the aeroservoelastic model; the tests included the grid loss condition, simulated by abruptly setting the control torque to zero, but were conducted in steady wind for the reason noted above. Next, we used the experimentally measured response to calibrate the mathematical model of the machine, achieving a good match between simulated and measured responses. To accurately capture peak loads, the model tuning phase highlighted the importance of a correct setting of the aerodynamic parameters at unusual angles of attack, achieved during this maneuver but otherwise seldom encountered in other operating conditions. Finally, we used the validated mathematical model to simulate shutdown maneuvers, this time including gusts, verifying in this more complete case the load reduction capability of the modified pitch profiles.

In an industrial design environment, these steps should be followed by up-scaling and the study and optimization of the pitch profile for the full scale machine, something that can be done more effectively and with greater confidence once a study as the one conducted here on the scaled model has been completed. In fact, such a study can help determine the level of confidence with which a mathematical model is capable of simulating the transient physical processes that take place during these extreme maneuvers. Furthermore, it also highlights which are the critical modeling aspects of a given class of problems, which in this case involved the airfoil aerodynamics at negative angles of attack. Clearly, similar conclusions would be very hard and expensive to achieve by using full scale field testing, also because of the uncertainty related to the testing conditions.

3.2.1. *Open-loop pitch profile optimization*

Not much literature seems to exist on the problem of optimizing the pitch profile during an emergency shutdown. For example, the patent described in Svendsen and Hammerum (2010) illustrates a pitch control strategy, based on rotor acceleration measurements, to optimally brake the wind turbine during emergencies. A general approach to the problem of reducing emergency-related envelope loads was described in Guerinoni (2013). In that work, a constrained optimal control formulation is used for automatically computing the best possible open-loop pitch profile during a shutdown. The solution is obtained by minimizing peak loads during the breaking maneuver over a variety of wind conditions and fault time instants, subjected to constraints that ensure an upper limit to the rotor overspeed and avoid to pointlessly push the peak loads too much below the next dominating ones. Although we were unable to use that approach here for property right issues, we consider in the following a simpler approach used in that same work to generate good quality initial guesses to the optimal control problem.

The standard max-pitch-rate policy used during an emergency shutdown can be expressed as

$$\beta(t) = \beta(t_f) + (t - t_f)\dot{\beta}_{\max}, \tag{8}$$

for $t > t_f$, where t_f is the instant when the fault occurs, while $\dot{\beta}_{\max}$ is the maximum achievable constant pitch rate. A better solution can be based on the idea of using a simple PD controller to generate the pitch profile by feeding back the fore-aft tower base

bending moment, which is the load that should be reduced. Since pitching during an emergency should be typically conducted in open loop, given that feedback measurements might not be available, the solution generated by the PD controller during simulations is not used directly, but it is employed for defining the open-loop policy effectively used during a real shutdown, as explained next.

Based on this idea, the modified pitch profile is defined as

$$\beta(t) = \beta(t_f) + (t - t_f)\dot{\beta}_c + \beta_{\mathrm{PD}}(t), \tag{9}$$

where $\dot{\beta}_c < \dot{\beta}_{\max}$ is a constant pitch rate, while β_{PD} is an additional feedback-generated term computed as

$$\beta_{\mathrm{PD}}(t) = K_P(M_{fa} - M^*_{fa}) + K_D\dot{M}_{fa}, \tag{10}$$

where M_{fa} is the tower base fore-aft bending moment, $(\cdot)^*$ indicates a reference value, and K_P and K_D are the proportional and derivative gains, respectively.

Fig. 12 shows simulation results for the rotor speed (at left) and tower base fore-aft bending moment (at right) during emergency maneuvers with the nominal pitch profile of Eq. (8) and the ones defined by Eqs. (9) and (10). As expected, it appears that one can readily trade an increase in rotor over-speed with a reduction of the peak load during the springing forward of the machine, generated by a rapid decrease and inversion of the rotor thrust caused by the aggressive pitch-to-feather of the blades.

Based on these results, one can try to identify an open-loop pitch profile. Being used in open-loop, the profile has to be unique for all emergencies, and therefore must be defined by considering multiple closed-loop solutions of the kind expressed by Eqs. (9) and (10). One simple approach to this problem is to define the shutdown profile as

$$\beta(t) = \beta(t_f) + (t - t_f)\dot{\beta}_c + \beta_{\mathrm{OL}}(t), \tag{11}$$

where the open-loop correction term approximating the effect of the closed-loop PD controller is the following parametric sinusoid:

$$\beta_{\mathrm{OL}}(t) = -\beta_a \sin(\omega_{\mathrm{OL}}(t - t_{\mathrm{OL}})), \quad t \in \left[t_{\mathrm{OL}}, t_{\mathrm{OL}} + \frac{\pi}{\omega}\right]. \tag{12}$$

The unknown to-be-defined parameters are represented by the amplitude β_a, the time shift t_{OL} and the pulsation ω_{OL}. It was found that to effectively cover the entire operating range of the machine, two time shifts are necessary, i.e. t^{II}_{OL} in region II (partial load) for $V \le V_r$ and t^{III}_{OL} in region III (full load) for $V > V_r$. The unknown parameters $\boldsymbol{p} = (\beta_a, \omega_{\mathrm{OL}}, t^{II}_{\mathrm{OL}}, t^{III}_{\mathrm{OL}})^T$ are computed by fitting the sinusoid given by Eq. (12) to N different shutdown time histories computed by the method of Eqs. (9) and (10) in a given range of wind speeds and for a given maximum pitch rate $\dot{\beta}_c$. The fitting can be performed by solving the following optimization problem:

$$\boldsymbol{p}^* = \arg\min_{\boldsymbol{p}} J, \quad J = \sum_{i=1}^{N} \int_{t_f}^{t_0^{(i)}} (\beta_{\mathrm{OL}}(t) - \beta^{(i)}_{\mathrm{PD}}(t))^2 \, \mathrm{d}t. \tag{13}$$

Since the goal of the procedure is the reduction of the negative peak of the tower fore-aft bending moment, which takes place during the first forward oscillation of the machine after the beginning of the maneuver, the cost function J of the optimization problem is only computed from the fault time t_f until $t_0^{(i)}$, which is the first instant when $\beta^{(i)}_{\mathrm{PD}}$ becomes null.

Open-loop pitch profiles, identified in this way, were implemented onboard the supervisory control system of the wind turbine model, and tested in the wind tunnel.

3.2.2. Experimental testing and model calibration

The different open-loop shutdown pitch policies listed in Table 2 were tested in the wind tunnel, for wind speeds varying between 6 and 12 m/s in steps of 2 m/s. The first three maneuvers are standard ones, as defined by Eq. (8), and differ in their maximum pitch rate, while the other two are based on the formulation of Eqs. (11) and (12) described in the previous section, and also differ in their steady-state pitch rates. The same maneuvers were simulated with the `Cp-Lambda` code.

Since the response of the machine during an emergency shutdown is significantly affected by the fore-aft behavior of the tower, the mathematical model was carefully verified in this respect. To this end, the stiffness and damping of the tower and of the balance placed at its foot were tuned with ad hoc measurements. Nonetheless, a comparison of the experimental and numerical results during shutdowns highlighted some remaining discrepancies. Such differences were traced back to uncertainties in the lift curve of the outer blade airfoil at negative angles of attack. Indeed, this region of the lift curve had been estimated using the method proposed in Moriarty and Hansen (2005), which is commonly adopted for extending airfoil polars to $\pm 180°$. Evidently, a more precise definition of the airfoil behavior as necessary in the present case.

To address this issue, the identification procedure described in Campagnolo (2012) was used to estimate the lift curve of the WM006 airfoil in the range $[-25, -1]°$, by minimizing the following cost function:

$$J = \sum_{i=1}^{M} \int_{t_f}^{t_0^{(i)}} ((\hat{\Omega}^{(i)}(t) - \check{\Omega}^{(i)}(t))^2 + w_M(\hat{M}^{(i)}_{fa}(t) - \check{M}^{(i)}_{fa}(t))^2) \, \mathrm{d}t, \tag{14}$$

where $\hat{(\cdot)}$ indicates a simulation quantity, $\check{(\cdot)}$ an experimentally measured one, and w_M is a weighing factor chosen so as to make the two terms dimensionally consistent. Only a subset M of the N

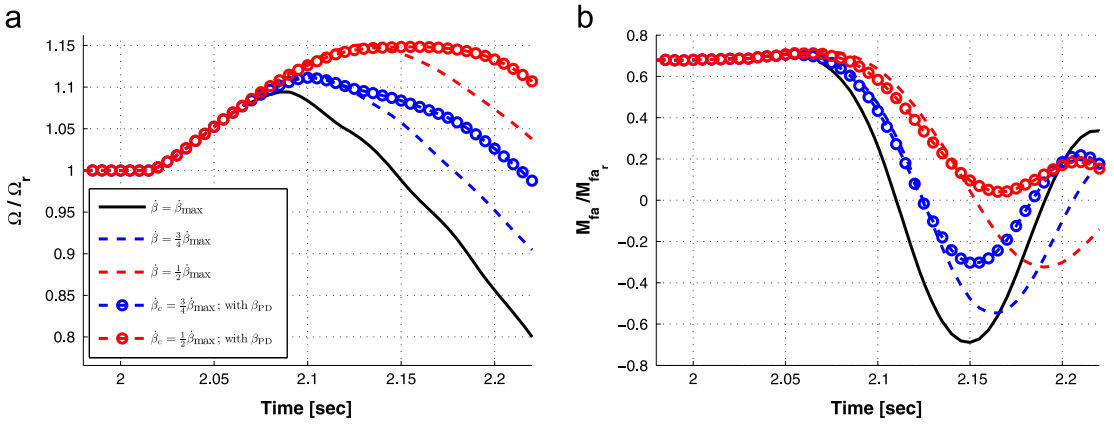

Fig. 12. Simulation results for the rotor speed (at left) and tower base fore-aft bending moment (at right) during emergency maneuvers with the pitch profiles defined by Eq. (8)–(10).

shutdowns was used for the tuning of the model, while the remaining ones were used for validating the results.

The nominal and identified lift curves are reported in Fig. 13; the latter exhibits a sharper stall and higher C_L values in the post-stall region than the former. The effect of the model calibration was to reduce the cost expressed by Eq. (14) by approximately 15%.

For the 8 m/s case using the pitch profile ID 1 from Table 2, a condition that was not used for model tuning, Fig. 14 shows the rotor speed (at left) and the tower base fore-aft bending moment (at right). The solid line represents the experimental results, the dashed line the simulation results prior to calibration, and finally the dash–dotted line the ones after calibration. It appears that, after tuning, the model shows an improved correlation with the experimentally measured data.

As the tuned mathematical model was shown to capture with good accuracy the response of the machine during this class of transient maneuvers, an optimization of the pitch profile was performed in the presence of a deterministic gust, as prescribed by the certification guidelines, considering here again the five possible pitch policies of Table 2.

Similar to what was previously done, feedback solutions were computed using the method of Eqs. (9) and (10) around rated wind speed, typically the most demanding case, for EOG conditions with simultaneous grid loss. Multiple cases were simulated, considering the fault to take place at different time instants, namely in correspondence to the gust lowest wind speed, maximum wind speed, and maximum wind speed rate of change. As before, the sinusoidal open-loop pitch profile defined by Eq. (12) was fitted to the closed-loop solutions, by solving optimization problem (13).

The best performing pitch profile was found to be the one with ID 4, which uses a 25% reduced maximum pitch rate and the optimized sinusoidal input. The use of this open-loop policy resulted in a reduction of the tower base fore-aft peak load of 20% and an increase in rotor over-speed of 10% with respect to the standard maximum pitch rate policy of Eq. (8).

A more thorough study should be conducted to prove the real robustness of the optimized policy, by verifying loads and over-speeds over a larger variety of conditions. In this regard, the approach of Guerinoni (2013) explicitly accounts for the entire operating envelope of the machine. Nonetheless, the example presented here serves well the purpose of illustrating the process of validation/calibration of the model from wind tunnel test data so as to ensure an appropriate level of fidelity for the specific problem at hand.

3.3. Active pitch/torque control

In this section we investigate active control applications that can be developed with the help of the experimental facility described in this work. At first we consider the design and tuning of a standard collective pitch and torque controller, that is used for the regulation of two wind turbine models operating in wake interference conditions. Next, we consider the alleviation of loads by the use of individual pitch control.

3.3.1. Control in wake interference conditions

At first we report on the development of collective pitch and torque control capabilities for the wind turbine model. The model controller, as for any wind turbine, should provide for the trimming of the machine depending on mean wind speed throughout the entire operating envelope, for the alleviation of loads due to

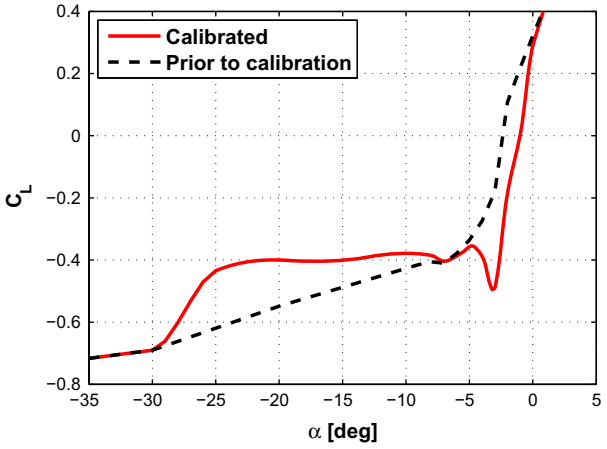

Fig. 13. Lift curve of the WM006 airfoil prior to and after calibration from shutdown test data.

Table 2
Maneuvers tested in the wind tunnel.

Maneuver ID	$\beta(t)$
1	$\beta(t_f)+(t-t_f)\dot{\beta}_{\max}$
2	$\beta(t_f)+(t-t_f)\frac{3}{4}\dot{\beta}_{\max}$
3	$\beta(t_f)+(t-t_f)\frac{1}{2}\dot{\beta}_{\max}$
4	$\beta(t_f)+(t-t_f)\frac{3}{4}\dot{\beta}_{\max}+\beta_{OL}(t)$
5	$\beta(t_f)+(t-t_f)\frac{1}{2}\dot{\beta}_{\max}+\beta_{OL}(t)$

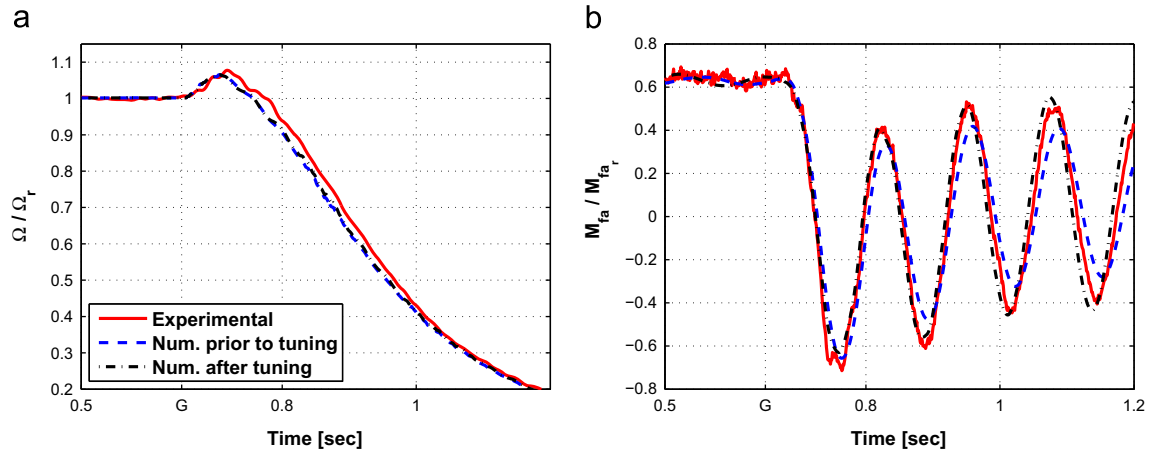

Fig. 14. Comparison among experimental and numerical solutions, prior to and after calibration, for the rotor speed (at left) and tower base fore-aft bending moment (at right).

wind fluctuations, and for good power output and power quality, targets that should be met while avoiding excessive actuator duty cycle (ADC, see Burton et al., 2001). Apart from such basic capabilities, the controller will also represent the baseline element of any other more advanced controller, as for example the individual blade pitch algorithms described in the next section.

These features not only allow for the basic control of the model, but also allow for the operation of two wind turbine models, one in the wake of the other. In fact, the testing of two wind turbines in wake effects is one of the unique characteristics of the present experimental facility, since it enables the study of wind turbine interactions and the testing of wind farm control algorithms. Although the dimensions of the model and of the wind tunnel allow only for two wind turbines to be simultaneously tested, this setup still captures the essence of the couplings that take place within a wind farm, i.e. the reduced speed and increased turbulence experienced by the downstream machine, and the dynamic changes of these parameters that follow from a change in the trim set point of the upstream wind turbine. Most literature on wind farm control uses either very simplified wind farm interaction models (Marden et al., 2009), which might not be very accurate, or very sophisticated CFD-based ones (Fleming et al., 2013), which are extremely demanding from a computational point of view. On the other hand, the present experimental facility, limited to two wind turbines, allows for a rapid, low cost and high fidelity testing of control algorithms, a capability that we intend to exploit in the near future.

We consider a classical collective pitch and torque PI controller, as described in Bossanyi (2000) and references therein. The implementation uses a torque look-up table for maximizing power output in region II, and a PI collective blade pitch controller for limiting power output to its rated value in region III (Bossanyi, 2000). The model wind turbine presents a transition region II½ (Bottasso et al., 2012) between partial and full power, where the rotor speed is constant and equal to its rated value, but power output is still below rated; a torque PI controller is used to handle this transition region.

The torque PI controller uses as its lower limit the optimal torque given by

$$T_{g_{\text{opt}}} = \frac{1}{2}\rho A R^3 \frac{C_{P_{\max}}}{\lambda^3_{C_{P_{\max}}}} \Omega^2, \tag{15}$$

and the rated generator torque as its upper limit, this in turn ensuring that the torque loop actively controls the wind turbine only in region II½. In region II, the rotor speed is lower than its nominal value, so the torque PI controller operates on its lower limit (the optimal torque of Eq. (15)), thereby ensuring an optimal energy conversion. In region III, the rotor speed cannot be maintained to its nominal value only by the generator torque, so the torque PI controller saturates to its upper limit, while the pitch PI controller maintains nominal rotor speed by setting the rotor blade pitch. A lower limit on the pitch PI is set to the optimal pitch angles in regions II and II½, which are readily determined from the C_P–λ–β curves; in turn, this ensures that the pitch loop actively controls the wind turbine only in region III. Switching between regions is done only based on wind turbine states — rotor speed, blade pitch angle and generator torque — so that there is no need to use wind speed measurements, except for the possible scheduling of control gains.

The collective pitch-torque algorithm was used for controlling two identical models (the upstream one being named WTM1, and the downstream one WTM2) in full-wake interference conditions, with the setup shown in Fig. 15. The regulation trajectory (Bottasso et al., 2012) was traced off-line, using the wind tunnel measured C_P–λ–β curves, while the controller gains were set and verified by hardware-in-the-loop tests performed on the back-to-back test bench.

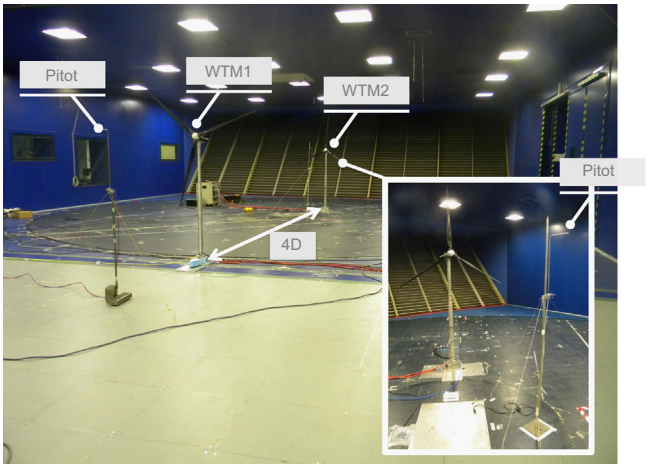

Fig. 15. Setup for the full-wake control tests.

Hub-height wind speeds V were measured approximately one diameter in front of each model by using `MENSOR CPT-6100 FS.=0.36PSI` and `DRUCK LPM9481 FS.=5mbar` Pitot transducers. Tests were performed at several wind speeds, with V_{WTM1} varying in the range [4.7, 10] m/s. The lower wind speed was selected to avoid having WTM2 operating in too low a win speed, which would further compromise Reynolds and hence aerodynamic performance.

Fig. 16 shows at left the hub-height wake deficit at the Pitot tube of the downstream wind turbine WTM2, as a function of the hub-height wind speed measured at the Pitot tube of the upstream machine WTM1. The plot includes horizontal and vertical error bars, computed as prescribed by the international standard (ISO, 2008, Annex G) and accounting for uncertainties due to flow turbulence, pitot tube misalignment and accuracy of the transducers. The same picture on the right shows the rotor speed (at top) and the output power of the two machines (at bottom). Notice how the wake deficit trend agrees with the WTM2 power output, which reaches rated at a wind speed of about 9 m/s, while the rotor speed plot shows that region II½ is reached for the downstream machine around 6.3 m/s.

Fig. 17 reports at left the measured thrust C_F and power C_P coefficients of the two machines. The plot shows the good trimming ability of the controller, being the power and thrust of the two models quite similar to each other for the same TSR. The small discrepancies observed in region II½ and III are probably due to the wind speed values used for data reduction; indeed, the Pitot transducers provide a local hub-height flow speed that probably underestimates the global wake deficit felt by the entire rotor.

For WTM2, Fig. 17 shows at right the distribution, as a function of hub-height wind speed, of rotor speed and power standard deviations, respectively noted σ_Ω and σ_P, and of the ADC, computed as

$$\text{ADC} = \frac{1}{T}\int_0^T \frac{|\dot{\beta}(t)|}{\dot{\beta}_{\max}}\,\mathrm{d}t. \tag{16}$$

The controller appears to be able to guarantee small rotor speed fluctuations in the entire operating region. Power quality and ADC trends are consistent with those measured on real machines, with the exception of the ADC values in region II, where pitch control appears to be a bit too active, a problem that can possibly be corrected by a better tuning of the gains.

3.3.2. *Individual pitch control*

By pitching the blades individually, the control activity can be tailored to the local wind experienced by each blade, with potential significant reductions of the periodic loads due to

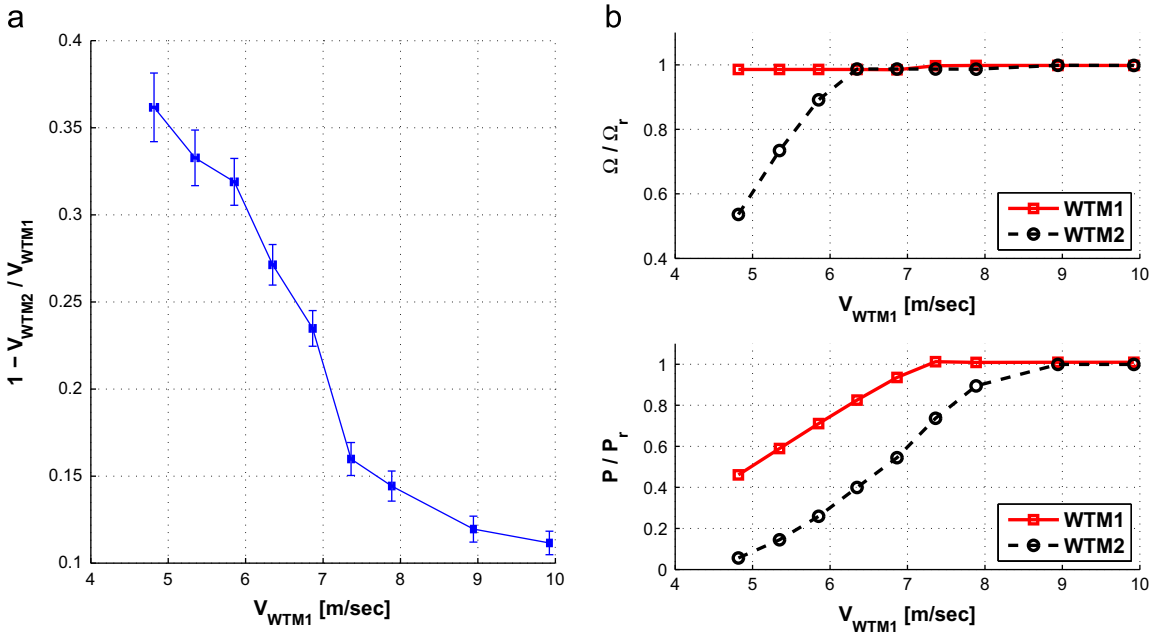

Fig. 16. Wake deficit (at left) and (at right) rotor speed (top) and power output (bottom) of the two wind turbines.

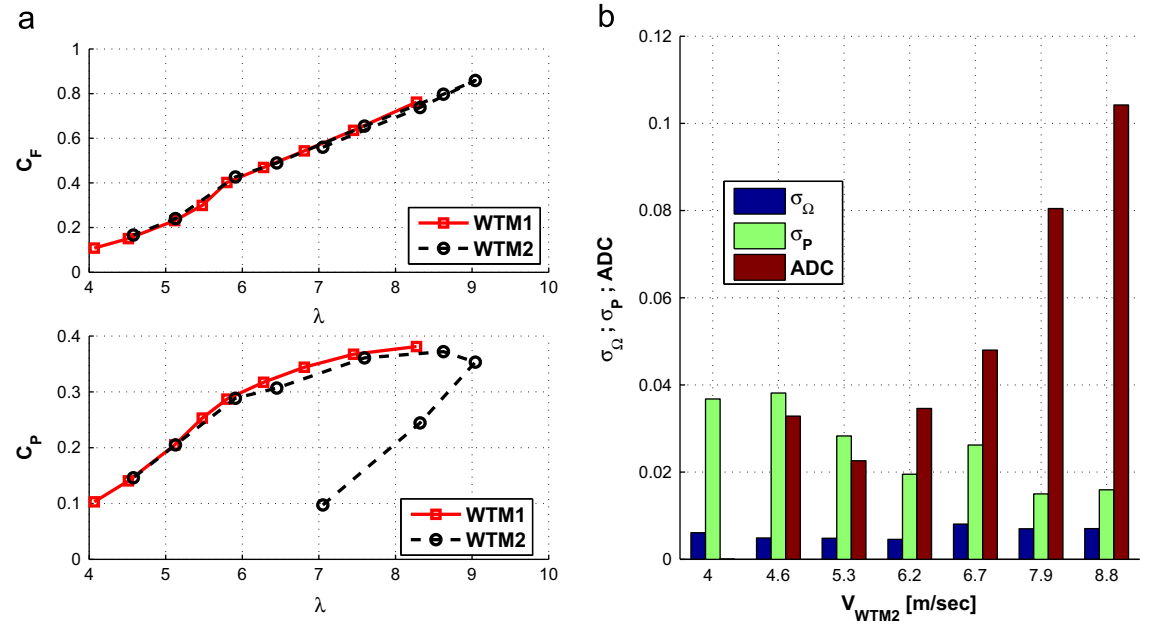

Fig. 17. Thrust (top left) and power (bottom left) coefficients for varying TSR, and (at right) rotor speed standard deviation σ_Ω, power standard deviation σ_P and ADC vs. hub-height wind speed for the downstream wind turbine.

non-uniform and non-axial flow conditions, as well as of the stochastic disturbances due to turbulence (see Bottasso et al., 2013, and references therein). IPC can be implemented as an additional layer that augments an underlying collective pitch and torque controller, whose role is the regulation of the machine around a set-point and the reaction to gusts. Typical IPC implementations primarily target 1P load harmonics in the rotating system, an effect that translates into load reductions at 0P in the fixed one. The working principle is to Coleman transform the blade loads, which has the effect of promoting 1P rotating harmonics to 0P stationary ones, that are in turn quenched by two PI controllers, one for each axis of the fixed reference frame, whose outputs are finally back-Coleman transformed to produce the pitch inputs to the blades (Bossanyi, 2003; Bossanyi et al., 2010).

IPC controllers targeting higher harmonic loads have also been proposed, either by using higher order Coleman transformations (van Engelen, 2006), or through optimal control approaches in the frequency domain (Bottasso et al., 2013).

In this work, single and higher harmonic IPC controllers were developed, by augmenting the collective pitch and torque controller described in the previous section. The controllers make use of the rotating shaft bending moments measured by strain gages. Apart from this difference, the singe harmonic IPC is essentially the classical formulation of Bossanyi (2003), which is typically based on blade load measurements. The higher harmonic implementation is on the other hand a variation on the one of van Engelen (2006), that accounts for the use of rotating shaft loads. Similarly to the 1P case, higher order transformations are used for

promoting higher order rotating harmonics to 0P stationary ones, so that even in this case PI controllers can be used for their reduction and the consequent generation of higher harmonic pitch inputs by back-transformation. Further details on the present formulation are given in Petrović and Campagnolo (2013)

Due to the high speed of the rotor, and consequent high frequency of the IPC controller, a possibly significant coupling between axes in the transformed coordinate system might be expected (Jelavić et al., 2010). To correct for this effect, which could degrade performance, a steady state coupling model was experimentally identified by recording load harmonics caused by prescribed harmonic variations of blade pitch, and then used for decoupling.

Tests were conducted by using two models in half-wake interference conditions, obtained by laterally displacing of about one rotor diameter the downstream wind turbine with respect to the upstream one. The highly non-uniform flow conditions experienced by the downstream machine induce loads with a wide spectrum, which makes it possible to verify the performance of the IPC algorithms. Three different controllers were used: the sole collective pitch controller, IPC targeting 1P loads (termed IPC-1P), and the higher harmonic IPC controller targeting 1P and 2P loads (termed IPC-1P2P).

For one of the experimental tests conducted with the upstream wind turbine operating in region II½, Fig. 18 reports time histories of measured rotating shaft bending components and blade pitch angles. At the beginning, IPC-1P2P is active. Then the higher harmonic feature is deactivated, resulting in the IPC-1P algorithm. Finally, the IPC controller is turned off, and the sole collective pitch and torque trimmer is operating. The figure clearly shows how load oscillations increase as the individual pitch activity is progressively decreased.

Fig. 19 summarizes the results in the frequency domain. The figure shows at left rotating shaft harmonics, at center blade pitch harmonics, and at right power harmonics. From the collective case, it appears that shaft loads have significant harmonics up to 2P, as expected, for the wake of the upstream machine impinges on half of the rotor of the downstream one. The IPC-1P controller nicely reduces 1P harmonics, as expected, but has also a beneficial effect at 2P, while the IPC-1P2P controller has an even more effective load reduction capability, enabled by the 2P pitch activity shown by the mid plot. It is important to stress that the load reductions achieved by the IPC controllers are obtained without affecting power production, as shown in the right plot.

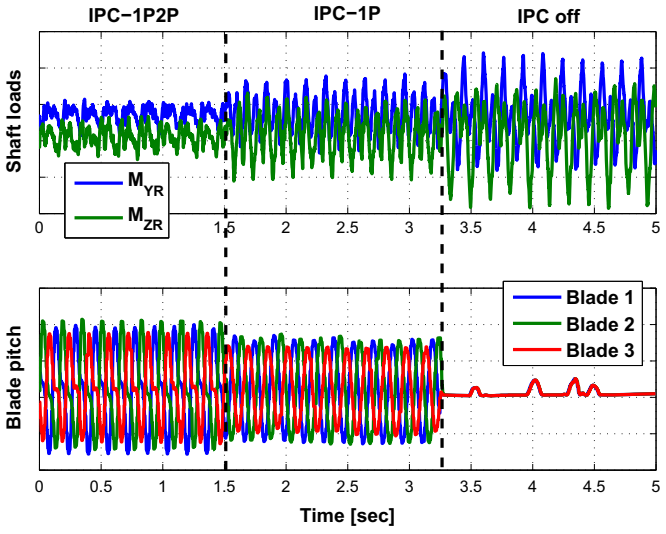

Fig. 18. Rotating shaft bending components (at top) and blade pitch activity (at bottom) for the downstream wind turbine operating in half-wake interference conditions.

4. Conclusions

The paper has described a novel experimental facility designed to expand the scope of wind tunnel testing of wind turbines beyond the domain of aerodynamics. This has been motivated by the fact that simulation is the key enabler of the design and optimization of wind energy systems, while model validation and calibration is the key enabler that ensures the reliability of predictions generated by simulation models. Although wind tunnel testing cannot exactly reproduce full-scale conditions nor can it substitute field-testing, it may nonetheless play an important role in the validation/tuning of models and in the evaluation of new concepts and ideas. By this work, we have tried to make a

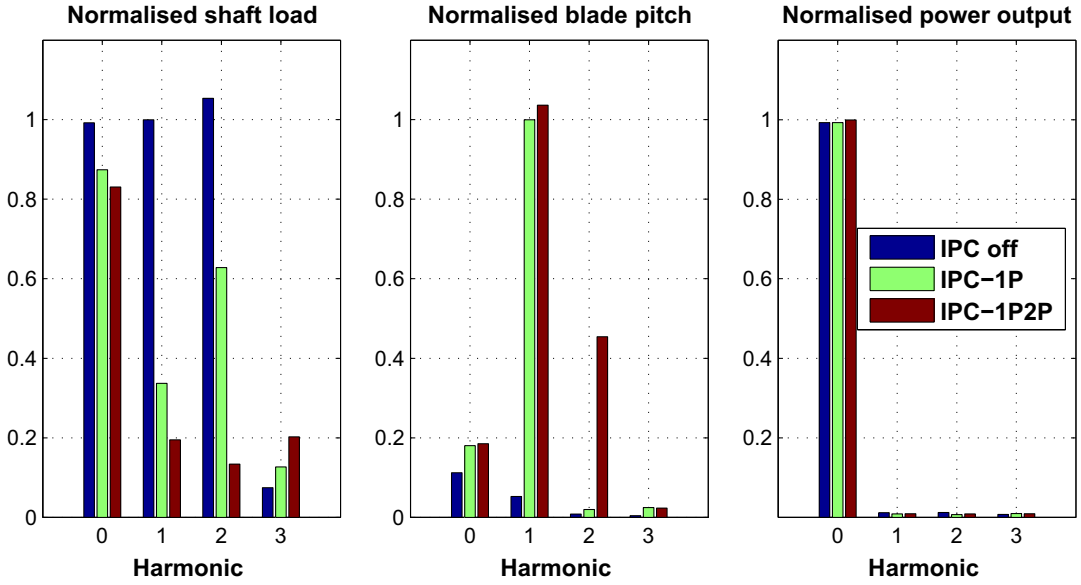

Fig. 19. Performance of the collective and IPC controllers for the downstream wind turbine operating in half-wake interference conditions.

step towards the building of a better understanding of the full potential of wind tunnel testing in these new application areas.

A novel aeroelastically scaled model has been described, featuring active individual pitch and torque control. The model has been used for conducting a number of non-aerodynamic and non-standard experiments, which have included open and closed-loop control, and the validation of control-support technologies. The new experimental facility was proven capable of effectively supporting the applications areas it was designed for, exhibiting a good robustness and availability throughout many hours and days of testing.

Clearly, the model has some limitations, primarily due to the inability to match the Reynolds number, resulting in a reduced power coefficient. Although care has been exercised to try to mitigate the effects of a substantially reduced Reynolds by using suitable airfoils equipped with transition strips, this problem is one of the prices to pay in exchange for the benefits offered by wind tunnel testing.

It should be noted that none of the examples described in the paper is significantly affected by the lower power coefficient. In fact, a reduced power means that rotor in-plane forces are smaller; however, since thrust is very well matched, out-of-plane forces are well represented on the scaled model. The wind misalignment observer is little affected by this problem, as the reconstruction of the wind direction is primarily driven by the flap response, which is accurate for the reasons noted above (in addition to the matching of the Lock number). Furthermore, the emergency shutdown case is dominated by the thrust behavior, which induces the large tower base moments that are the objective of the investigation. Similarly, the load alleviation demonstrated by the use of IPC is also primarily due to the reduction of flap loads.

Other problems might be more sensitive to the in-plane behavior of the rotor, or to effects due to the reduced Reynolds, so that the use of the experimental facility for the validation of models or the testing of technologies should be made with attention to the specific goals of any given investigation activity. For example, Reynolds-dependent unsteady aerodynamic effects will change between the full scale and the scaled wind turbines. Notwithstanding these limitations, several other key parameters are correctly captured. In fact, the matching of the lower frequency Campbell diagram ensures a realistic vibratory response. The matching of the Lock number means that the ratio of aerodynamic and inertial forces is accurately represented. The exact matching of TSR ensures that the aerodynamic kinematics (blade angles of attack, near wake geometry) are precisely represented. The shape of the power and thrust coefficients vs. TSR and blade pitch are also very well matched, with the sole exception that the former is lower; however, the curves have very similar shapes and the maximum power coefficient is located at the same TSR value of the full scale case. This means that the shape of the regulation trajectory (the loci of points in the power/thrust-TSR-pitch space occupied by the machine for varying wind conditions) is essentially the same, which implies that controllers governing the full scale and scaled machine will have essentially the same behavior and settings. Finally, the wake structure is well represented, as the speed deficit is very realistic due to the good matching of thrust, and Reynolds plays only a marginal role in the downstream location of the vortex breakdown.

Apart from what was shown here, the model has the potential for further expansions in other application areas. Studies on wind turbine interactions and wind farm control can be supported with the present setup, limited to two machines; a small array of wind turbines could be realized by designing a model with a smaller rotor diameter. Furthermore, the passive mitigation of loads by the use of bend-twist coupling can be studied by the design of blades featuring suitable aeroelastically tailored characteristics, again with the goal of verifying the ability of simulation codes to capture all relevant effects. Another direction of possible future development is in the area of off-shore wind, where important aeroelastic, stability and control problems come from the coupling of the machine with a floating support structure. To enable such applications, one can mount the present model on an actuated moving platform, whose motion is either prescribed or co-simulated on the basis of a suitable model of the "wet" part of the machine, or directly mount the model on a floating platform for testing in a tank. We plan to explore these and other exciting possibilities in the near future.

Acknowledgments

The present project is funded by Vestas Wind Systems A/S. V. Petrović acknowledges the support of "ACROSS — Centre of Research Excellence for Advanced Cooperative Systems" (FP7 Project no. 285939), who funded his visit to the Politecnico di Milano to cooperate on the project. The authors wish to thank Bachmann Electronic GmbH, for their partial financial support and technical contribution to the development of the real-time control system, and M. Bassetti, P. Bettini, M. Biava, S. Calovi, S. Cacciola, F. Cadei, G. Campanardi, M. Capponi, G. Galetto, D. Grassi, M. Mauri, S. Rota, G. Sala, C. Simeone, S. Spinelli, A. Zasso of the Politecnico di Milano for numerous technical contributions in the development of the experimental facility.

References

Althaus, D., 1988. ProfilPolaren für den Modellflung, Band 1. Necktar-Verlag, Vs-Villingen. Institut für Aerodynamik und Gasdynamik der Universität Stuttgart (in German).

Bahaj, A.S., Molland, A.F., Chaplin, J.R., Batten, W.M.J., 2007. Power and thrust measurements of marine current turbines under various hydrodynamic flow conditions in a cavitation tunnel and a towing tank. Renew. Energy 32 (3), 407–426.

Barenblatt, G.I., 1996. Scaling, Self-Similarity, and Intermediate Asymptotics: Dimensional Analysis and Intermediate Asymptotics. Cambridge Texts in Applied Mathematics. Cambridge University Press, UK.

Bauchau, O.A., Bottasso, C.L., Nikishkov, Y.G., 2001. Modeling rotorcraft dynamics with finite element multibody procedures. Math. Comput. Model. 33, 1113–1137.

Bossanyi, E., 2000. The design of closed loop controllers for wind turbines. Wind Energy 3, 149–163.

Bossanyi, E., 2003. Individual blade pitch control for load reduction. Wind Energy 6, 119–128.

Bossanyi, E., Wright, A., Fleming, P., 2010. Further progress with field testing of individual pitch control. In: Proceedings of the European Wind Energy Conference 2010, Warsaw, Poland.

Bottasso, C.L., Croce, A., 2009–2013. `Cp-Lambda` User's Manual. Dipartimento di Ingegneria Aerospaziale, Politecnico di Milano.

Bottasso, C.L., Croce, A., Riboldi, C.E.D., Nam, Y., 2012. Power curve tracking in the presence of a tip speed constraint. Renew. Energy 40, 1–12.

Bottasso, C.L., Croce, A., Riboldi, C.E.D., Nam, Y., 2013. Multi-layer control architecture for the reduction of deterministic and non-deterministic loads on wind turbines. Renew. Energy 51, 159–169.

Bottasso, C.L., Riboldi, C.E.D., 2014. Estimation of wind misalignment and vertical shear from blade loads. Renew. Energy 62, 293–302.

Braslow, A.L., Knox, E.C., 1958. Simplified Method for Determination of Critical Height of Distributed Roughness Particles for Boundary-Layer Transition at Mach Numbers from 0 to 5. Technical Report TN-4363, NACA.

Buckingham, E., 1914. On physically similar systems; illustrations of the use of dimensional equations. Phys. Rev. 4, 345–376.

Burton, T., Sharpe, D., Jankings, N., Bossanyi, E., 2001. Wind Energy Handbook. John Wiley & Sons, Chichester, West Sussex, England.

Campagnolo, F., 2013. Wind Tunnel Testing of Scaled Wind Turbine Models: Aerodynamics and Beyond (Ph.D. thesis). Dipartimento di Ingegneria Aerospaziale, Politecnico di Milano.

Fleming, P., Lee, S., Churchfield, M., Scholbrock, A., Michalakes, J., Johnson, K., Moriarty, P., Gebraad, P., van Wingerden, J., 2013. The SOWFA super-controller: a high-fidelity tool for evaluating wind plant control approaches. In: Proceedings of the EWEA 2013 Annual Event, Vienna, Austria.

Giavotto, V., Borri, M., Mantegazza, P., Ghiringhelli, G., 1983. Anisotropic beam theory and applications. Comput. Struct. 16, 403–413.

Guerinoni, L., 2013. Ottimizzazione di procedure di frenata di emergenza per aerogeneratori (Master's thesis). Dipartimento di Ingegneria Aerospaziale, Politecnico di Milano (in Italian).

Hand, M.M., Simms, D.A., Fingersh, L.J., Jager, D.W., Cotrell, J.R., Schreck, S., Larwood, S.M., 2001. Unsteady Aerodynamics Experiment Phase VI: Wind Tunnel Test Configurations and Available Data Campaigns. Technical Report NREL/TP-500-29955, NREL National Renewable Energy Laboratory, USA.

Hill, K.O., Meltz, G., 1997. Fiber Bragg grating technology fundamentals and overview. J. Lightwave Technol. 15, 1263–1276.

International Standard IEC, 2005. Wind Turbines—Part 1: Design Requirements. IEC 61400-1, Ed. 3.0.

International Standard ISO, 2008. Measurement of Fluid Flow in Closed Conduits—Velocity Area Method using Pitot Static Tubes, second ed. ISO 3966.

Jelavić, M., Petrović, V., Perić, N., 2010. Estimation based individual pitch control of wind turbine. Automatika—J. Control Meas. Electron. Comput. Commun. 51, 181–192.

Jonkman, J., Butterfield, S., Musial, W., Scott, G., 2009. Definition of a 5-MW Reference Wind Turbine for Offshore System Development. Technical Report NREL/TP-500-38060, National Renewable Energy Laboratory (NREL), Golden, CO, USA.

Marden, J.R., Ruben, S.D., Pao, L.Y., 2009. A model-free approach to wind farm control using game theoretic methods. In: Proceedings of the 50th IEEE Conference on Decision and Control, Orlando, FL, USA, vol. 129, pp. 584–596.

Moriarty, P.J., Hansen, A.C., 2005. AeroDyn Theory Manual. National Renewable Energy Laboratory, January.

Ogata, K., 1997. Modern Control Engineering. Prentice-Hall, Upper Saddle River, New Jersey, USA.

Oku, Y., Kump, K., Bruce, E.N., Cherniack, N.S., Altose, M.D., Whale, J., Papadopoulos, K.H., Anderson, C.G., Helmis, C.G., Skyner, D.J., 1996. A study of the near wake structure of a wind turbine comparing measurements from laboratory and full-scale experiments. Sol. Energy 56, 621–633.

Olesen, N.A., 2009. Personal communication. Vestas Wind Systems A/S. Aarhus, Denmark.

Petrović, V., Campagnolo, F., 2013. Experimental validation of higher harmonic control using shaft load measurements. In: Proceedings of the European Control Conference 2013, Zurich, Switzerland, July.

Schepers, J.G., Snel, H., 207. Model Experiments in Controlled Conditions—Final Report. Technical Report ECN-E-07-042, ECN Wind Energy, The Netherlands.

Snel, H., Schepers, J.G., Montgomerie, B., 2007. The MEXICO project (Model EXperiments In Controlled cOnditions): the database and first results of data processing and interpretation. J. Phys.: Conf. Ser. 75.

Svendsen, R., Hammerum, K., 2010. Control of Rotor During a Stop Process of a Wind Turbine. US Patent Application No. 2010/0196 156.

van Engelen, T.G., 2006. Design model and load reduction assessment for multi-rotational mode individual pitch control (higher harmonics control). In: Proceedings of the European Wind Energy Conference 2006, Athens, Greece.

Vermeer, L.J., Sørensen, J.N., Crespo, A., 2003. Wind turbine wake aerodynamics. Prog. Aerosp. Sci. 39, 467–510.

Ziegler, J.G., Nichols, N.B., 1942. Optimum settings for automatic controllers. Trans. ASME 64, 759–768.